Zhang *et al.*
Cell Communication and Signaling (2024) 22:437
https://doi.org/10.1186/s12964-024-01813-5

Cell Communication and Signaling

RESEARCH

Open Access

A novel amphiphilic squalene-based compound with open-chain polyethers reduces malignant melanoma metastasis in-vitro and in-vivo

Yaman Zhang[1], Meriem Bejaoui[2,3], Tran Ngoc Linh[2], Takashi Arimura[2] and Hiroko Isoda[1,2,3,4*]

Abstract

Squalene (SQ) is a well-known antioxidant and anti-inflammatory agent that provides promising anti-aging and UV-protective roles on human skin. However, its strong hydrophobic nature, accompanied by issues such as poor solubility and limited tissue permeation, has created challenges for scientists to investigate its untapped potential in more complex conditions, including cancer progression. The present study assessed the potent anti-metastatic properties of a newly synthesized amphiphilic ethylene glycol SQ derivative (SQ-diEG) in melanoma, the most fatal skin cancer. In vitro and in vivo experiments have discovered that SQ-diEG may exert its potential on melanoma malignancy through the mitochondria-mediated caspase activation apoptotic signaling pathway. The potent anti-metastatic effect of SQ-diEG was observed in vitro using highly proliferative and aggressive melanoma cells. Administration of SQ-diEG (25 mg/kg) significantly decreased the tumor burden on the lung and inhibited the metastasis-associated proteins and gene markers in B16F10 lung colonization mice model. Furthermore, global gene profiling also revealed a promising role of SQ-diEG in tumor microenvironment. We anticipated that the amphiphilic nature of the SQ compound bearing ethylene glycol oligomers could potentially augment its ability to reach the pathology site, thus enhancing its therapeutic potential in melanoma.

Keywords Melanoma, Metastasis, Squalene, Ethylene glycol, Tumor microenvironment

Introduction

Malignant melanoma can be highly metastatic and invasive with the highest mortality among skin cancers [1]. Extensive metastasis can result in serious, permanent damage to organs as well as psychological damage to the affected patients.

Metastatic spread of melanoma requires multiple conditions: 1. Melanoma cells must undergo large morphological changes, called epithelial-mesenchymal transition (EMT), to form aggressive phenotypes, so they can cross the basement membrane of extracellular matrix (ECM) and invade through the connective tissues with the coordination of adhesion molecules (e.g. integrins) [2]. 2. The released melanoma cells will go through a harsh battle of

*Correspondence:
Hiroko Isoda
isoda.hiroko.ga@u.tsukuba.ac.jp
[1] Tsukuba Life Science Innovation Program (T-LSI), University of Tsukuba, Tsukuba, Japan
[2] Open Innovation Laboratory for Food and Medicinal Resource Engineering (FoodMed-OIL), National Institute of Advanced Industrial Science and Technology (AIST), Tsukuba, Japan
[3] Alliance for Research On the Mediterranean and North Africa (ARENA), University of Tsukuba, Tsukuba, Japan
[4] Institution of Life and Environmental Sciences, University of Tsukuba, Tsukuba, Japan

survival with immune cells in the circulation [3]. 3. The survived cells will colonize on the appropriate site [4]. 4. Cells on the periphery work to recruit additional oxygen and nutrient sources, forming new blood vessels to support tumor proliferation [5]. Notably, the Matrix Metalloproteinase (MMP) families play a variety of roles within the tumor microenvironment (TME, a heterogeneous ecosystem composed of cancer cells, immune cells, the ECM, etc.), especially on the degradation of type IV collagen (the major component of ECM structure), indicating their significance as cancer markers, which explains the intense interest in these proteins as a desirable target for cancer treatment [6, 7].

Due to the high propensity of melanoma tumors metastasizing to distinct organs, current therapeutic strategies still cannot meet the rising demand for patients. Nowadays, the use of natural compounds in cancers, including their synthetic derivatives, either as primary or adjunctive therapy has become a spotlight in response to the patient's wishes to pursue a safer and sustainable therapeutic effect [8]. A number of natural-derived agents have discovered to prompt melanoma apoptosis, anti-proliferation, anti-migration, and regulate immune functions within TME [9–12]. More importantly, multi-target activity of natural compounds, which means one compound being able to shoot multiple pharmacological bullets at the same time, could be a promising approach to target a large network of proteins and genes that are involved in the development and the spreading of the melanoma while exhibiting a much lower possibility of side effects compared to the single target drugs [13].

Squalene (SQ) is a naturally occurring substance which was originally isolated from shark liver oil but also can be obtained from many renewable sources aiming to achieve the highest yields with lower costs, such as vegetables (e.g. olive oil, soybean oil, grape seed oil) and microorganisms (e.g. microalgae *Aurantiochytrium* sp.) [14]. Topical application of SQ has shown excellent effect on UV radiation protection and skin lubrication with no harm to the human skin [15]. Although several experimental and animal evidence suggests that SQ possesses anti-cancer properties [16, 17], its strong hydrophobic nature, which inevitably accompanied with the issues, such as poor solubility, limited cell permeation, and low bioavailability in living organisms, has created challenges for scientists to investigate its underestimated potentials in more complex conditions, such as cancer metastasis. Hence, to overcome this barrier, a novel SQ receptor, 2-[2-(2-hydroxyethoxy)ethoxy]-3-hydroxysqualene (SQ-diEG) which bearing ethylene glycol (EG) oligomers, and forming vesicle-like particles to facilitate the cell membrane penetration, was synthesized [18], and then used in this current research as a potent molecule candidate against melanoma progression. We aimed to elucidate the potent anti-metastatic effect of SQ-diEG in-vitro and in-vivo and to reveal its mechanism of action via global gene expression analysis.

Materials and methods

Chemicals

SQ-diEG was first synthesized from 2,3-epoxysqualene and characterized by means of Rf, FT-IR, 1H NMR, ^{13}C NMR, and HR-MS as described in the previous study [18]. We stated that the Purity (%) of SQ-diEG used in this study was Purity (%) = 98.9 wt%. The stock solution of SQ-diEG was first prepared in dimethyl sulfoxide (DMSO) (Wako, JP) and stored in 4 °C until use. The stock solution was then diluted in the fresh growth medium to obtain 0.1% of DMSO for cell treatment or diluted it with saline solution to reach a maximum dose of 5% DMSO v/v for animal experiment. Dacarbazine (DTIC) (Sigma, USA) was received in powder form and prepared in DMSO for stock solution. The stock solution was stored in 4 °C and further diluted in saline reach a maximum dose of 5% DMSO v/v for animal administration.

Declarations of the animal research

Eight per group, six-weeks old male C57BL/6 J mice, total 40 mice (Charles River Laboratories, JP) were housed individually in polycarbonate cage under 12 h light/dark cycle condition. Mice were allowed to access to food and water freely for 7 days acclimatization before the start of experiment. We strictly followed the guidelines of the University of Tsukuba's Regulation of Animal Experiments and all the experiments were approved by the University of Tsukuba's Committee on Animal Care and Use (No. 22–465).

Cell culture

B16F10 murine melanoma cells (RIKEN, JP) were cultured in Roswell Park Memorial Institute Medium (RPMI 1640) (Gibco, NY) which supplemented with 10% fetal bovine serum (FBS) (Gibco, NY) and 1% Penicillin/Streptomycin (Gibco, NY) and incubated at 37 °C in a humidified atmosphere of 5% CO2. SK-MEL-28 human skin melanoma cells (ATCC, USA) were cultured in Eagle's Minimum Essential Medium (EMEM) (ATCC, USA) supplemented with 10% fetal bovine serum (FBS) (Gibco, NY) and 1% Penicillin/Streptomycin (Gibco, NY) and incubated at 37 °C in a humidified atmosphere of 5% CO2. For animal intravenous injection, 2×10^5 cells/ml B16F10 cells were resuspended in saline solution and then aggregated cells were removed using 79-µm-cell strainer (Falcon, USA).

Cell proliferation assay

The cytotoxicity of SQ-diEG were investigated by using 3-(4, 5-dimethylthiazol-2-yl)-2, 5-diphenyltetrazolium bromide (MTT assay) (Dojindo, JP). B16F10 cells and SK-MEL-28 cells were seeded onto 96-well plates at a concentration of 3×10^4 cells/well. After overnight incubation at 37 °C in a humidified atmosphere of 5% CO2, cells were treated with SQ-diEG at various concentrations for 48 h and 72 h. Then 5 mg/ml MTT solution was added to each well and further incubated for 6 h. Finally, the cells were treated with 10% sodium dodecyl sulfate (SDS) to completely dissolve the formazan crystals. After overnight incubation, the cell viability was measured by a microplate reader at 570 nm absorbance. Results were calculated by average of three independent trials.

Immunofluorescence

The cellular proliferation of B1F10 cells was determined by the immunodetection of a proliferation marker, Ki67 (Abcam, USA). B16F10 cells were seeded on to 4-well LabTek Chamber Slides (Sigma, USA) at a concentration of 3×10^4 cells/well. After overnight incubation, cells were treated without or with SQ-diEG for 24 or 48 h. Then cells were washed with 0.1% v/v Triton X-100/ phosphate-buffered saline (PBS) (Sigma, USA) and fixed with 4% paraformaldehyde (PFA) under agitation at room temperature (RT). Cells were treated with the primary antibody Ki67 (1:10,000) in blocking buffer (1.5 g of bovine serum albumin (BSA), 50 ml of PBS, and 100 µl of Triton X-100) and incubated overnight at 4 °C under agitation. Then, the cells were immersed with the secondary antibody Alex 488-conjugated anti-rabbit (Abcam, USA) (1:10,000) and incubated at RT for 1 h. Finally, the cells were mounted with DAPI solution (Sigma, USA) and visualized under a Leica DMI-4000B fluorescence microscope (Leica Microsystems, Germany). Photographs including three fields of each sample well were taken. The number of positive Ki67 cells/well was quantified by ImageJ and results were confirmed by three independent trials.

Cell cycle analysis

B16F10 cells were seeded onto 6-well plate at a concentration of 5×10^4 cells/well and then incubated overnight. The cells were treated without or with SQ-diEG and incubated for 24, 48, and 72 h. The cells were harvested by trypsination (0.25% trypsin⁄ 0.02% EDTA in PBS; Gibco, NY) and were diluted with growth medium to obtain 1×10^6 cells/ml. Cells were washed once with 1×PBS and then fixed by 70% ice cold ethanol. After incubation overnight at 4ºC, cells were washed once with 1×PBS and then samples were transferred into the wells of a 96-well-round bottom. The 200 µl of propidium iodide (PI) cell cycle staining reagent (Luminex Corporation, USA) which used to label cellular DNA was added to each well and mixed well by pipetting up and down for several times. Then the plate was incubated at RT shielding away from light for 30 min. Data were acquired on the Guava PCA-96 using CytoSoft™ software. Statistics of CytoSoft histogram for each cell population, including M1 (G0/G1), M2 (S), M3 (G2/M), showed percent total, PM1 mean, median and %CV fluorescence intensity. Average of gated % Positive representing the average percentages for the M1, M2, and M3 were calculated by three independent trials.

Measurement of mitochondria membrane potential

The active mitochondria in SK-MEL-28 cells were label and localized with MitoTracker™ Red CMXRos staining kit (Molecular Probes, CA). The 1 mM stock solution was prepared in high quality DMSO and then diluted to the 100 nM in growth medium before use. The SK-MEL-28 cells were seeded on to 4-well LabTek Chamber Slides (Sigma, USA) at a concentration of 3×10^4 cells/ well. After overnight incubation, cells were treated without or with SQ-diEG for 48 h. When cells have reached the desired confluency, the medium was removed and cells were stained with the 100 nM solution containing MitoTracker red probe for 45 min at RT. After incubation, cells were washed carefully with the growth medium and then fixed with 4% PFA for 15 min at RT. After fixation, cells were rinsed with growth medium carefully and then mounted with DAPI solution (Sigma, USA) Finally, the cells were visualized under a Leica DMI-4000B fluorescence microscope (Leica Microsystems, Germany). Photographs including three fields of each sample well were taken and results were confirmed by three independent trials.

Cell migration assay

Cell migration and movement was analyzed by wound healing assay. B16F10 and SK-MEL-28 cells were seeded onto 6-well plates at a concentration of 1×10^5 cells/well and incubated overnight. When the cells reach 90% confluency, a scratch was carefully made in the middle of the confluent monolayer by using a sterile white tip. Then old medium was removed and cells were washed with 1×PBS. After the unattached cells were removed, cells were treated without or with SQ-diEG. Finally, cells were observed under a contrast microscope (Leica Microsystems, Germany) and photographs of each well were taken after the desired treatment hours. The results were quantified using ImageJ by three independent trials.

Transwell invasion assay

The cell invasion of B16F10 and SK-MEL-28 cells were evaluated using a Boyden chamber model (Abcam, USA). Firstly, the cells were starved for 24 h in a serum-free medium. Then the top chamber was coated with collagen for 2 h and after washed with 1 M Tris. The cells were collected into pellet and resuspended in a serum free medium. In the bottom chambers, the medium containing desired chemoattractant (10% FBS) were added. The medium containing without the chemoattractant was added in the control chamber and the medium containing Control Invasion Inducer was added to the positive control chamber. On the other hand, in the top chambers, 2.3×10^5 cells were seeded onto the top chamber in a serum-free medium. Then the medium without or with SQ-diEG was treated to the cells and mixed gently. The cell invasion chamber was incubated at 37 °C in CO2 incubator. After incubation for 24 h, non-invasive cells left in the top chambers were removed by cotton swab. Highly invasive cells on the outside layer of the inserts were fixed by 4% PFA and the cell nuclei were stained with DAPI. Finally, the cells were visualized under a Leica DMI-4000B fluorescence microscope (Leica Microsystems, Germany). Photographs of each sample chamber were taken and the number of invasive cells was quantified by ImageJ and results were confirmed by three independent trials.

Clonogenic assay

B16F10 and SK-MEL-28 cells were seeded onto 6-well plates at a concentration of 5×10^4 cells/ml and then treated without or with SQ-diEG for 5 days until visible colonies formed. Then cells were washed carefully with ice-cold 1×PBS. The cells were fixed with ice-cold methanol for 10 min and stained with 0.5% crystal violet solution for a 10 min incubation at RT. Then cells were rinsed carefully with distilled water for several times. The cells were dried at RT for 1 h and finally photographs were obtained by a contrast microscope (Leica Microsystems, Germany). The results were quantified using ImageJ by three independent trials.

Tumorigenesis assays

Total 40 C57BL/6 J mice (8 mice/treatment group) were randomly divided into five groups: Control: (-) B16F10 injected and water treated; Model: (+) B16F10 injected and water treated; Positive control: (+) B16F10 injected and DTIC treated (70 mg/kg/day); Treatment: (+) B16F10 injected and SQ-diEG treated (5 mg/kg/day); Treatment: (+) B16F10 injected and SQ-diEG treated (25 mg/kg/day). After one week of acclimatization, mice tail was wiped with 70% ethanol or warm water aiming to see the mice lateral tail veins clearly and then lateral tail veins were injected with B16F10 cells (2×10^5 tumor cells in 100 µl PBS, 0.2 ml/mouse). The day after B16F10 injection, mice were orally administered every morning, to ensure that each animal receive the exact dosage corresponding to each animal's body weight for a total treatment of 20 days. Food and water were given as described above during the experimental period. The day after the last oral administration, the mice were sacrificed using the cervical spine dislocation method and the lungs were collected, washed, the number of lung tumor colonies was counted, then quick frozen in liquid nitrogen and finally stored at -80 °C for further experiments.

Immunohistochemistry

The melanoma lung tissue was embedded in optimum cutting temperature (OCT) compound and kept in -80 °C until use. The OCT-embedded lung sections were cut at a thickness of 10 µm and fixed with 4% PFA (Sigma, USA). Firstly, the sections were washed several times in PBS, 0.1% v/v Triton X-100/PBS (Sigma, USA), and 20 mM of glycine/PBS. Then the sections were incubated in blocking solution for 1 h at RT (0.2 g of bovine serum albumin (BSA), 400 µl of gelatin, 18.4 ml of PBS, 500 µl of normal donkey serum, and 500 µl of normal goat serum), the sections were further incubated with mouse anti-MMP2 (Abcam, USA) and rabbit anti-MMP9 (Abcam, USA) overnight at 4 °C in a wet chamber. On the next day, the lung sections were washed again as previously described and then incubated with secondary antibody, Alexa Fluor 488-conjugated anti-mouse (Abcam, USA) and Alexa 647-conjugated anti-rabbit (Abcam, USA) at 1:200 ratio in blocking solution for 1 h under RT. After the incubation and washing, the sections were dried and sealed for 15 min and mounted in DAPI solution (Sigma, USA), and visualized under a Leica DMI-4000B fluorescence microscope (Leica Microsystems, Germany). Results were quantified by ImageJ and confirmed by three independent trials.

RNA extraction and quantitative real-time PCR

The total RNA of melanoma lung tissue and melanoma cells was extracted using Isogen (Nippon Gene Ltd, JP) according to the manufacturer's directions. The final RNA concentration was assessed using a NanoDrop 2000 spectrophotometer. The effect of SQ-diEG on gene expression was assessed by using TaqMan Gene Expression Master Mix (Applied Biosystems, USA) and TaqMan primers (Applied Biosystems, USA) with the following thermal cycling protocol: (95 °C, 10 min, 40 cycles of 95 °C for 15 s, and 60 °C for 1 min). Specific primers used in this study were *Ikbke, Hmox1, Sqstm1, Mgp, Nnmt*, *Myc*, *Prdm1*, *Bax, Bak, Bcl-xL, Tp53, Atf4* and *Gapdh* (as an internal reference control). Then data were analyzed

using 7500 Fast Real-time PCR System with 7500 software version 2.0.5 (Applied Biosystems, USA). Results were calculated by the average of three independent trials.

DNA microarray analysis

Microarray analysis was performed on the Affymetrix's GeneAtlas® System (Affymetrix Inc, USA). Total RNA samples were prepared and quantified as mentioned above. Then the amplified and purified antisense RNA (complementary RNA or cRNAs) were generated and purified by using purification beads on a magnetic stand. The sense-strand cDNA samples were synthesized, purified, fragmented, and labeled following the manufacturer's instructions. After, cartridge array hybridization was performed on the GeneAtlas® instrument. We used the mouse genome array strips which were then washed and stained with the GeneAtlas® Fluidics Station. Finally, data and figures were generated by AGCC scan using the GeneAtlas® Imaging Station.

We used multiple online bioinformatic software for microarray analysis. Enriched gene ontology of biological process (BP) was analyzed using DAVID Bioinformatics: (https://david.ncifcrf.gov/) [19]. Circos plot and hierarchical cluster plot were analyzed through Metascape (http://metascape.org/) [20]. The generic PPI network was analyzed via NetworkAnalyst tool (version 4.3.2). Bubble plots were generated by SRPLOT (https://www.bioinformatics.com.cn/srplot). Venn diagram was generated through (https://bioinformatics.psb.ugent.be/webtools/Venn/) and heatmap was generated by MORPHEUS (https://software.broadinstitute.org/morpheus/).

Measurement of Caspase 3/7 activity

The activity of Caspase 3/7 was examined by using Caspase-Glo® 3/7 Assay kit (Promega, USA) according to the instructions. Briefly, B16F10 and SK-MEL-28 cells were seeded onto 6-well plate at a concentration of 5×10^4 cells/well and then incubated overnight. The cells were treated without or with SQ-diEG and then incubated for 6, 12, 24, 48 h. The Caspase-Glo® 3/7 Reagent was prepared by transferring the Caspase-Glo® 3/7 Buffer into the Caspase-Glo® 3/7 Substrate, mixed well until the substrate is thoroughly dissolved. Then 100 µl of Caspase-Glo® 3/7 Reagent was added to each well of a white-walled 96-well plate containing 100 µl of blank, untreated control cells or SQ-diEG treated cells in culture medium, total of 200 µl. The plate was gently agitated at 300–500 rpm for 30 s and incubate for 3 h at RT. Finally reading of the luminescence of each sample well was measured by a microplate reader.

Statistical analysis

All the data were analyzed and expressed as mean ± standard deviations (SD) ($n=3$). The level of significance between two value sets (ctrl cells vs. treated cells) was determined by student's t test: $^{*}P<0.05$, $^{**}P<0.01$, $^{***}P<0.0001$. For DNA microarray, the Transcriptome Analysis Console (TAC) software (ThermoFisher Scientific, USA) was used to analyze the data by running comparisons of gene expression in treated and ctrl cells based on SST-RMA algorithm. Level of significance between groups were assessed by using one-way between-subject ANOVA (paired) and genes which p value < 0.05 were considered as differentially expressed genes (DEGs).

Results

SQ-diEG affected the cellular proliferation of B16F10 cells and SK-MEL-28 cells

We first wanted to assess the direct role of SQ-diEG on aggressive melanoma cells (Fig. 1A). As rapid cell proliferation is one of the critical hallmarks of cancer development [21], we checked the effect of SQ -diEG on B16F10 cell proliferation. Therefore, cells were exposed to various concentrations (0, 2.5, 5, 10, 20, 40 µM) of SQ-diEG for 48 h and 72 h. The results revealed that SQ-diEG exhibited significant cytotoxic effect to the melanoma cells in a dose- and time-dependent manner (Fig. 1B), and SQ-diEG at a low dose (2.5 µM) and a high dose (40 µM) were used for further analysis. Further, the cellular proliferation rate of B16F10 cells upon SQ-diEG treatment was investigated by monitoring the expression of Ki67 which is a large nuclear protein expressed only in actively dividing cells, thus strongly related with the tumor cell proliferation and growth [22]. After the 24 h and 48 h

(See figure on next page.)

Fig. 1 SQ-diEG attenuated cellular proliferation in B16F10 cells and SK-MEL-28 cells. **A** The compound structure of 2-[2-(2-hydroxyethoxy) ethoxy]-3-hydroxysqualene (SQ-diEG). **B** The effect of SQ-diEG on B16F10 cell viability was measured by MTT assay. **C** Immunostaining of Ki67 in B16F10 cells. **D** The effect of SQ-diEG on cell cycle arrest in B16F10 cells after 24 h treatment. **E** The effect of SQ-diEG on cell cycle arrest in B16F10 cells after 48 h treatment. **F** The effect of SQ-diEG on cell cycle arrest in B16F10 cells after 72 h treatment. Cell distribution in cell cycle was expressed as % total (pink indicates G0/G1 phase, green indicates S phase, blue indicates G2/M phase). **G** The effect of SQ-diEG on SK-MEL-28 cell viability was measured by MTT assay. **H** MitoTracker Red CM-H2XRos staining of mitochondria in SK-MEL-28 cells. All the data were analyzed and expressed as mean ± standard deviations (SD) ($n=3$). The level of significance between two value sets (ctrl cells vs. treated cells) was determined by student's t test: $^{*}P<0.05$, $^{**}P<0.01$, $^{***}P<0.0001$

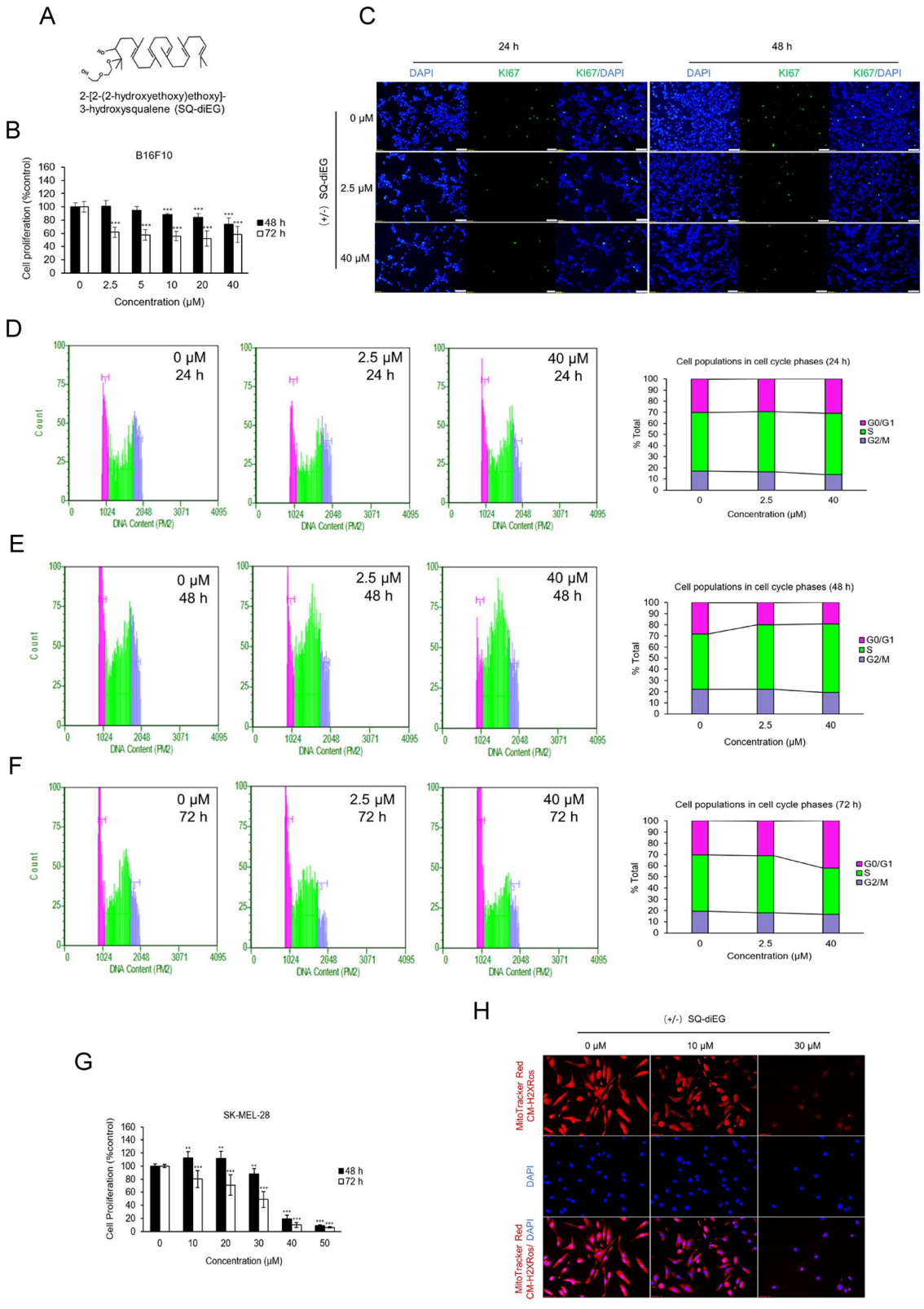

Fig. 1 (See legend on previous page.)

treatment of 2.5 and 40 μM SQ-diEG, immunofluorescence results suggested that the relative amount of Ki67 positive cells were significantly reduced at both concentrations, indicating that the cellular proliferation rate of B16F10 cells was suppressed by SQ-diEG (Fig. 1C, Fig. S1).

To gain more insight about whether low proliferation rate caused by SQ-diEG was correlated or not with cell cycle arrest, cell flow cytometric analysis was assessed. The DNA histogram results showed no significant change in cell cycle after 24 h treatment of SQ-diEG, but a slight trend of cell arrest was found in S phase (Fig. 1D). However, after 48 h treatment, a significant cell cycle arrest was observed in S phase (***P*-value, ctrl vs 40 μM (0.007) (Fig. 1E). Interestingly, a longer treatment (72 h) of 40 μM SQ-diEG indicated a significant cell arrest in early G0/G1 phase (***P*-value, ctrl vs. 40 μM (0.002), suggesting that SQ-diEG may exert damage to the B16F10 cells in a continuously manner, leading to a failure of cell cycle re-entry (Fig. 1F). Altogether, these data revealed that the low cellular proliferation of B16F10 cells after treated with SQ-diEG was correlated with the cell blocking in cell cycle stages. Specifically, the higher dose of SQ-diEG could persistently stress the B16F10 cells by inducing cell cycle arrest in S phase after 48 h, that will shift to G0/G1 phase arrest after 72 h treatment.

To confirm the potential impact of SQ-diEG on human melanoma cell proliferation, we treated SK-MEL-28 human melanoma skin cells with various concentrations of SQ-diEG. As expected, SQ-diEG also suggested considerable cytotoxic effect to the SK-MEL-28 cells and we used 10 μM and 30 μM for further validations (Fig. 1G). What's more, mitochondria are fundamental energy suppliers to fuel melanoma respiration and proliferation [23]. MitoTracker Red CM-H2XRos is used to stain mitochondria in actively respiring cells and its accumulation is dependent upon membrane potential [24]. Interestingly, we observed that SQ-diEG significantly suppressed the mitochondrial membrane potential (Δψm) in SK-MEL-28 cells after 48 h treatment, meaning that the cell respiration and cell proliferation activity were attenuated (Fig. 1H, Fig. S2).

Overall, these data revealed that SQ-diEG treatment induced a significant decrease in melanoma cell viability and proliferation, demonstrating that this compound, as a cytotoxic agent, possesses potent anti-melanoma activity.

SQ-diEG inhibited the melanoma metastatic-related activities in B16F10 and SK-MEL-28 cells

Widespread of metastasis is the leading cause of death in melanoma patients [1]. To further investigate the anti-metastatic activity of SQ-diEG on melanoma cells, directional cell migration was investigated by wound healing assay. The results indicated that the wound scratch established in the middle of the confluent monolayer was completely closed in the untreated control cells after 24 h. However, SQ-diEG significantly inhibited the B16F10 and SK-MEL-28 cell migration and movement in a dose- and time-dependently manner (Fig. 2A, B). The diminished cell aggressiveness to migrate through the semipermeable membrane in the Boyden chamber was also observed in both melanoma cell lines (Fig. 2C, D). In addition, clonogenic assay measures the ability of single cell to expand into large colony which is an important feature of metastatic cancer cells to occupy distant tissues [4]. We further confirmed that SQ-diEG observably restrained the B16F10 and SK-MEL-28 clonal expansion after 5 days treatment (Fig. 2E, F). Hence, these results demonstrated an anti-metastatic impact of SQ-diEG in melanoma cells.

SQ-diEG reduced the tumor burden on the lung along with the suppressed expression of melanoma metastatic-related markers

Despite the promising anti-metastatic-like effect of SQ-diEG in melanoma cells, we next aimed to evaluate the role of SQ-diEG on living organisms with functional immune responses. We assessed the potential of SQ-diEG on tumor colony expansion to distant organs, such as the lung, in the mice. The invasive B16F10 melanoma cells were delivered through the intravenous injection to create experimental metastatic foci. The circulating tumors were metastasized and colonized themselves on the lung after 20 days of oral administration with dacarbazine (DTIC, a chemotherapy medication for metastatic melanoma, positive control, 70 mg/kg/day), SQ-diEG (5 mg/kg/day) and SQ-diEG (25 mg/kg/day) (Fig. 3A). Our results suggested that no tumor nodes were found in the ctrl (-)B16F10 group, whereas a significant number of tumor nodes were found in the melanoma model (+)B16F10 groups. Notably, a significant reduction in the tumor nodes was observed in the DTIC treated group and 25 mg SQ-diEG treated group, suggesting that SQ-diEG possesses promising potential for the attenuation of tumor proliferation and colonization during the process of melanoma metastasis in vivo (Fig. 3B).

On the other hand, the contributions of gelatinases (MMP2 and MMP9) to tumor metastasis have been widely discussed. The MMP2 and MMP9 are crucial cancer biomarkers which play an active part in the degradation of ECM components, facilitating the primary tumors to metastasize [6], thus their related protein expression was checked. Results of OCT-embedded lung sections containing tumor edge indicated that the MMP2 and MMP9 expression of treated groups including DTIC

treated and SQ-diEG (5 mg and 25 mg) treated were significantly suppressed comparing to the model (+)B16F10 group (Fig. 3C, Fig. S3). We further checked the mRNA expression of various melanoma metastatic-associated markers via Rt-qPCR. For example, SQ-diEG significantly inhibited the gene expression of *Ikbke* (a novel oncogene in melanoma metastasis and in TME), *Hmox1* (a protumorigenic factor in melanoma proliferation), *Sqstm1* (a melanoma metastatic marker), *Mgp* (a mesenchymal gene and a pro-metastatic factor in many types of cancer including skin cancer), and *Nnmt* (a molecular biomarker in melanoma metastasis) (Fig. 3D-H). Altogether, these data proved that SQ-diEG plays a tumor suppressive role on melanoma proliferation, colonization and metastasis by downregulating the expression level of ECM degradation proteins and pro-metastatic factors.

SQ-diEG and DTIC showed different functions in melanoma tumor tissues

To understand the actual mechanism of SQ-diEG on melanoma progression, a whole-genome transcriptomic analysis by DNA microarray was carried out in melanoma lung tissues. We first assessed the variables and functions between the treatment groups, especially between the SQ-diEG treated and DTIC treated group. Results revealed the number and distribution of differentially expressed genes (DEGs) in each comparison group (Fig. 4A, B). In particular, total of 1356 genes were regulated in (-)B16F10 vs (+)B16F10 (melanoma model group), out of which 524 genes were upregulated and 832 were downregulated. A total of 1085 genes were regulated in DTIC vs (+)B16F10 group, out of which 500 genes were upregulated while 585 genes were downregulated. The treatment with 5 mg SQ-diEG, significantly modulated total 1209 genes, which 520 genes were upregulated and 689 genes were downregulated. For the 25 mg SQ-diEG treated group, total 1191 genes were regulated including 613 upregulated genes and 578 downregulated genes.

Next, the Circos plot showed the patterns and relationships between pairs of gene sets, which the identity of each gene set was encoded by the outside arc. The shared genes by multiple genes sets were encoded by dark orange color on the inside arc and the unique genes in a particular gene set was encoded by the light orange color on the inside arc. The purple ribbon connects the same gene that was shared by multiple gene lists, which means greater number of purple ribbons indicated the greater number of shared genes between the paired gene lists (Fig. 4C). Furthermore, we conducted functional across analysis to visually observe the similarities and differences of enriched clusters (gene ontologies (GOs), KEGG pathways, canonical pathways, hall mark gene sets, etc.) among treatment groups (Fig. 4D). Although some clusters, for example, detection of chemical stimulus, cellular response to cytokine stimulus, and cytokine signaling in immune system, were both enriched by SQ-diEG treated groups and DTIC group, many enrichments were lack in DTIC but unique in SQ-diEG treated, including VEGFA VEGFR2 signaling, adaptive immune system, transcriptional regulation by RUNX1, and cell morphogenesis. Thus, these data demonstrated that SQ-diEG may exert anti-metastatic effect on melanoma progression through a different mechanism than DTIC.

Discovery of similarities and differences in enriched gene ontologies between low-dose and high-dose SQ-diEG treated mice

Interestingly, heatmap also showed that interventions of the 5 mg and 25 mg SQ-diEG in melanoma mice might not be identical (Fig. 4D). Aiming to explore if any difference in low and high treatment of SQ-diEG, the significant DEGs were subjected to enriched gene ontology (GO) analysis for a detailed illustration of their regulation on biological processes (BP). Accordingly, in 5 mg SQ-diEG treatment group, that GOs linked with, for example, metabolic process (GO:0008152), cellular development process (GO:0048869), apoptotic process (GO:0006915), stress-related BP including the cellular response to reactive oxygen species (GO:0034614), and melanosome assembly (GO: 1903232) which related with the pigmentation, were upregulated upon low dose treatment of SQ-diEG. While some BPs, such as cell motility (GO:0048870), biological adhesion (GO:0022610), cell migration (GO:0016477), inflammatory response (GO:0006954) and positive regulation of angiogenesis (GO:0045766) which contribute to tumor progression by promoting cell invasiveness and angiogenesis, were

(See figure on next page.)

Fig. 2 SQ-diEG inhibited the metastatic potential in malignant melanoma cells. **A** The effect of SQ-diEG on cell movement and migration in B16F10 cells was measured by wound healing assay. **B** The effect of SQ-diEG on cell movement and migration in SK-MEL-28 cells was measured by wound healing assay. **C** The effect of SQ-diEG on cell invasion in B16F10 cells was measured by transwell assay. Invasion inducer was used as a positive control. **D** The effect of SQ-diEG on cell invasion in SK-MEL-28 cells was measured by transwell assay. Invasion inducer was used as a positive control. **E** The effect of SQ-diEG on colony formation in B16F10 cells. **F** The effect of SQ-diEG on colony formation in SK-MEL-28 cells. All the data were analyzed and expressed as mean ± standard deviations (SD) ($n = 3$). The level of significance between two value sets (ctrl cells vs. treated cells) was determined by student's t test: * $P < 0.05$, ** $P < 0.01$, *** $P < 0.0001$

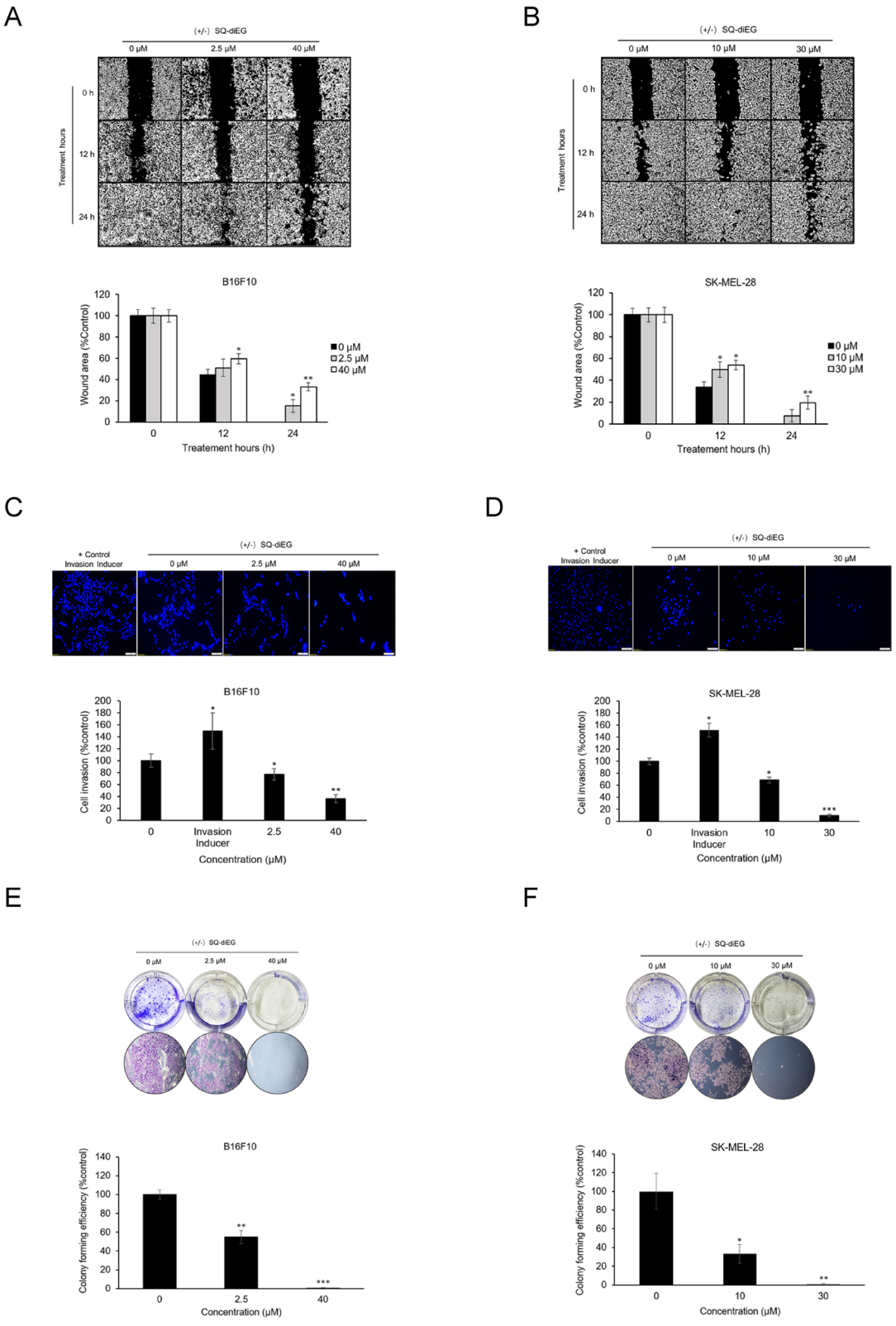

Fig. 2 (See legend on previous page.)

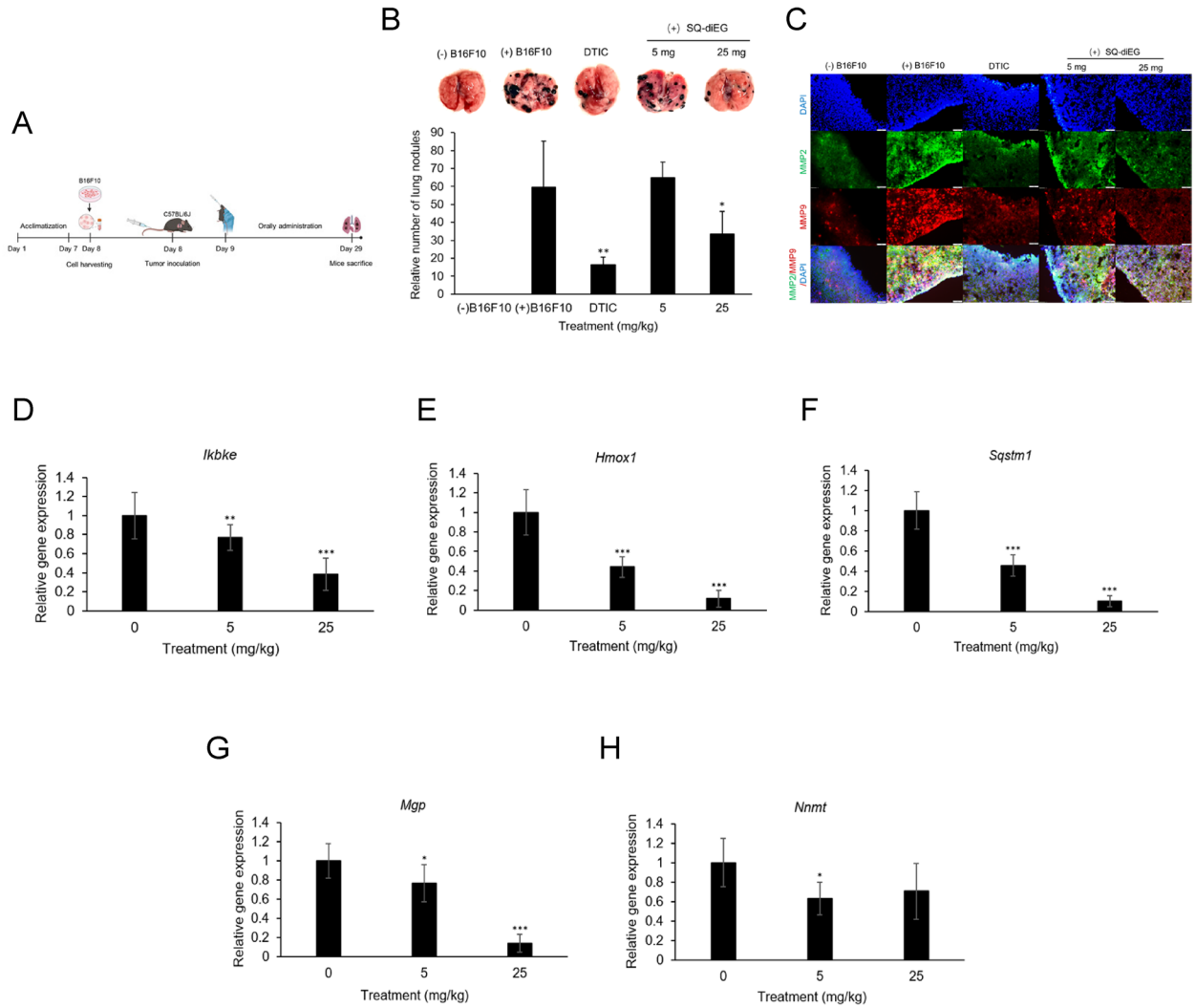

Fig. 3 SQ-diEG inhibited the melanoma colonization on the lung and suppressed the expression of melanoma metastatic-associated markers in mice. **A** The protocol of the performed animal experiment. Melanoma lung colonization mice model was established by I.V injection of B16F10 cells through the tail vein. Mice was orally treated with water, DTIC and SQ-diEG accordingly for 20 days. Upon sacrifice, the mice lung was washed and collected. The figure was created via BioRender tool and the agreement number of this publication is YV279AJAKI. **B** Photographs and counting of the number of melanoma nodules (tumors) on the lung. **C** Immunostaining of MMP2 and MMP9 expression in melanoma lung tissue. **D** The mRNA expression of melanoma metastatic-related gene marker, *Ikbke*. **E** The mRNA expression of melanoma metastatic-related gene marker, *Hmox1*. **F** The mRNA expression of melanoma metastatic-related gene marker, *Sqstm1*. **G** The mRNA expression of melanoma metastatic-related gene marker, *Mgp*. **H** The mRNA expression of melanoma metastatic-related gene marker, *Nnmt*. All the data were analyzed and expressed as mean ± standard deviations (SD) ($n = 3$). The level of significance between two value sets (ctrl cells vs. treated cells) was determined by student's t test: * $P < 0.05$, ** $P < 0.01$, *** $P < 0.0001$

shown to be significantly downregulated by 5 mg SQ-diEG (Fig. 5A). With the 25 mg treatment, GOs involved in, for example, metabolic process (GO: 008152), cellular component organization (GO: 0016043), positive regulation of response to DNA damage stimulus (GO: 2001022), positive regulation of extracellular matrix organization (GO: 1903055) and immune response related function including the neutrophil homeostasis (GO: 0001780), were upregulated. On the other hand, GOs correlated with the melanoma metastasis, for example, cell motility, migration, adhesion, proliferation, angiogenesis, and signaling related with the pro-tumorigenic TME including NF-kappaB signaling and integrin-mediated signaling, were significantly downregulated by 25 mg SQ-diEG (Fig. 5B).

Overall, both 5 mg and 25 mg SQ-diEG treatment repressed the GOs related to melanoma metastasis (cell motility, migration, adhesion, angiogenesis,

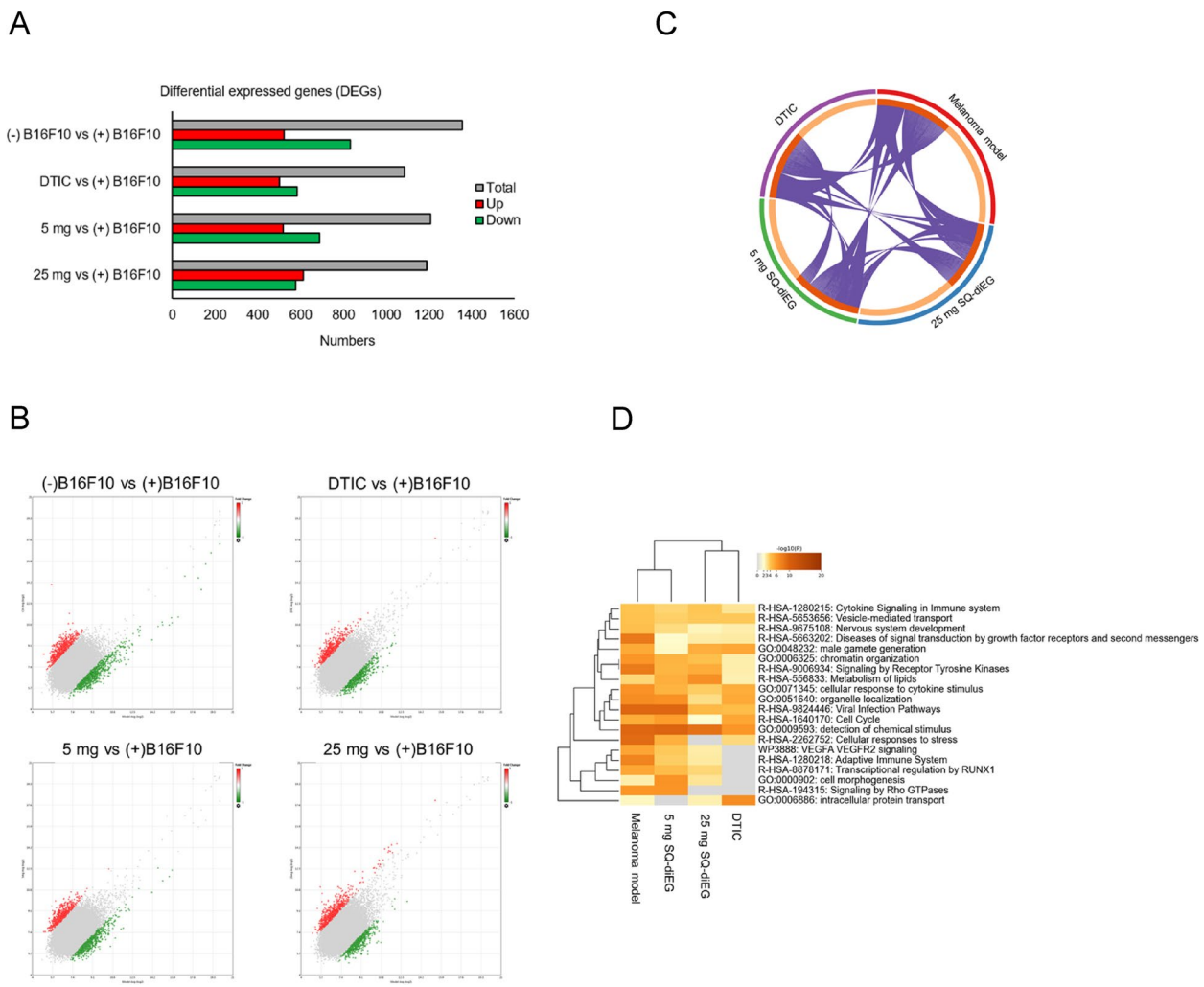

Fig. 4 Global gene expression profiling of SQ-diEG and DTIC. **A** Number of DEGs in treatment groups. Red color represents the upregulated DEGs. Green color represents the downregulated DEGs. Grey color represents total DEGs. **B** Distribution of the DEGs in scatter plot. X-axis and Y-axis represent the average signal intensity (log2). **C** Circos plot shows how genes from the input gene lists overlap. **D** Hierarchical cluster plot shows the enriched terms (can be GO/KEGG terms, canonical pathways, hall mark gene sets, etc.) across the treatment groups

inflammation, etc.) and upregulated the stress-stimulated BPs, such as cellular response to reactive oxygen species, apoptosis, and positive regulation of response to DNA damage stimulus. Nonetheless, 25 mg SQ-diEG enhanced the BP, positive regulation of extracellular matrix organization, suggesting that higher treatment of SQ-diEG may better participate in the construction of ECM components and regulation of ECM dynamics, which its dysregulation is one of the hallmarks of metastatic cancers [25].

(See figure on next page.)

Fig. 5 Functional comparison between the 5 mg and 25 mg SQ-diEG. **A** GO analysis shows the enriched BPs in 5 mg SQ-diEG treatment group. **B** GO analysis shows the enriched BPs in 25 mg SQ-diEG treatment group. Upper panel represents upregulated GOs. Down panel represents downregulated GOs. **C** The first-order generic PPI network in 5 mg SQ-diEG. **D** The first-order generic PPI network in 25 mg SQ-diEG. Red color represents upregulated protein seeds. Green color represents downregulated protein seeds. **E** Top 20 hub nodes. Upper panel represents top 20 hub nodes in 5 mg SQ-diEG. Down panel represents top 20 hub nodes in 25 mg SQ-diEG. **F** TF-gene interaction network in 5 mg SQ-diEG. **G** TF-gene interaction network in 25 mg SQ-diEG. Red color represents upregulated genes. Green color represents downregulated genes. Grey color represents TFs. **H** Validation of the mRNA expression of *Myc*. I. Validation of the mRNA expression of *Prdm1*. Values were analyzed and expressed as mean ± standard deviations (SD) ($n = 3$). The level of significance between two value sets (ctrl cells vs. treated cells) was determined by student's t test: * $P < 0.05$, ** $P < 0.01$, *** $P < 0.0001$

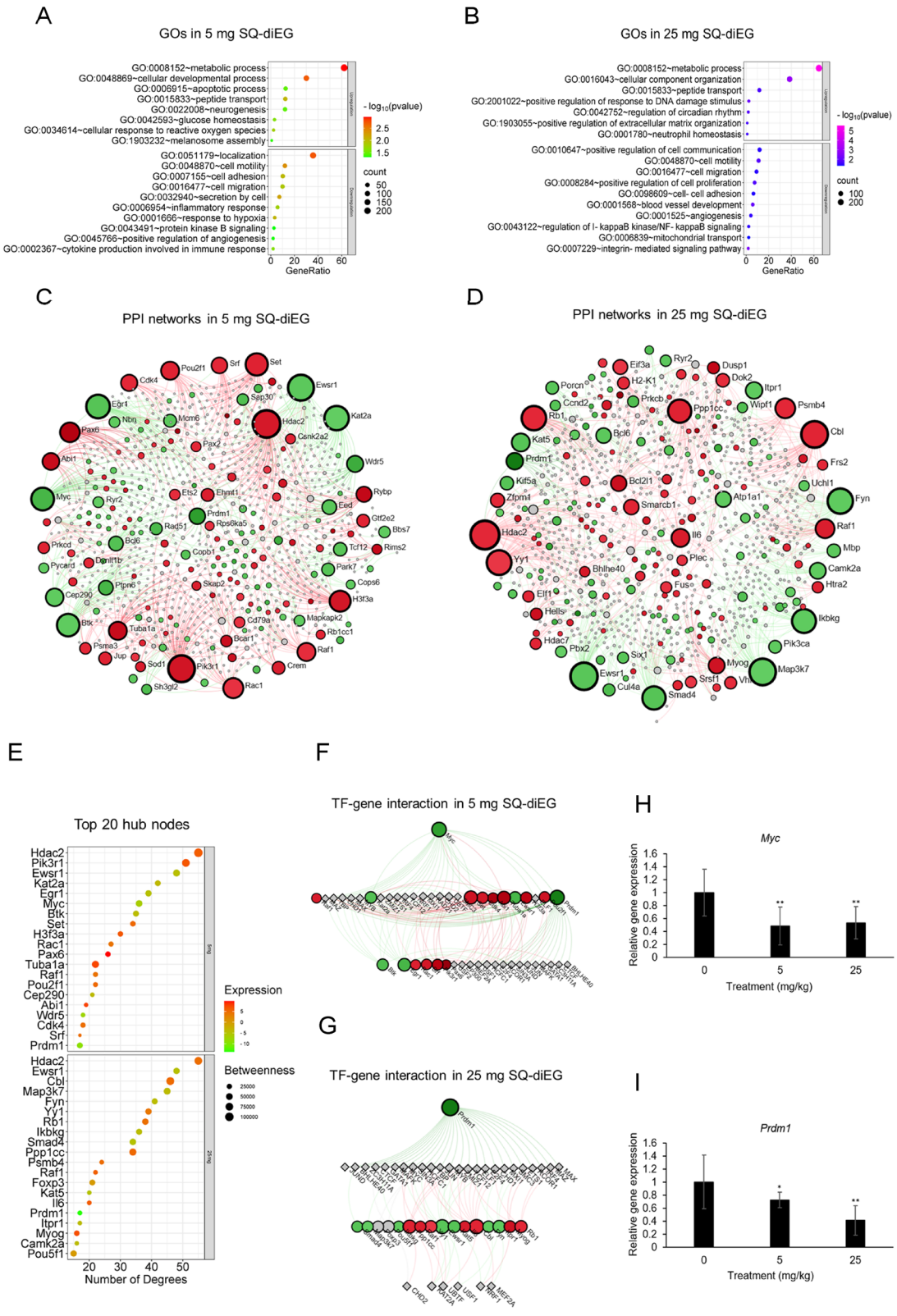

Fig. 5 (See legend on previous page.)

Variations in protein–protein interactions between low-dose and high-dose SQ-diEG treated mice

Protein–protein interaction (PPI) network analysis further predicted that 5 mg SQ-diEG positively affected the pathways, including B cell receptor signaling pathway (Rac1, Pik3r1, Cd79a, Raf1), T cell receptor signaling pathway (Pik3r1, Raf1, Cdk4), natural killer cell mediated cytotoxicity (Rac1, Pik3r1, Raf1), autophagy (Rb1cc1, Pik3r1, Raf1, Prkcd, Ctsb), apoptosis (Pik3r1, Raf1, Ctsb, Tuba1a), and longevity regulating pathway (Hdac2, Sod1, Pik3r1). While pathways, transcriptional misregulation in cancer (Ewsr1, Bcl6, Myc, Tspan7) and cellular senescence (Myc, Mapkapk2, Capn2, Nbn), were negatively regulated upon 5 mg SQ-diEG treatment (Fig. 5C). Comparatively, higher dose (25 mg) of SQ-diEG stimulated the pathways including apoptosis (Htra2, Bcl2l1) and natural killer cell mediated cytotoxicity (Klrk1, H2-K1, Raf1), and downregulated pathways correlated with the facilitation of the melanoma metastasis, for example, focal adhesion (Fyn, Prkcb, Itgav, Pik3ca, Ccnd2, Itga2b), chemokine signaling pathway (Prkcb, Ccr6, Ikbkg, Pik3ca, Pik3r5, Ccr2), HIF-1 signaling pathway (Camk2a, Prkcb, Pik3ca, Ldha), inflammatory mediator regulation of TRP channels (Camk2a, Prkcb, Itpr1, Pik3ca), proteoglycans in cancer (Camk2a, Prkcb, Itgav, Itpr1, Pik3ca), ECM-receptor interaction (Itgav, Cd47, Itga2b), PI3K-Akt signaling pathway (Itgav, Ikbkg, Pik3ca, Ccnd2, Pik3r5, Itga2b), transcriptional misregulation in cancer (Ewsr1, Bcl6, Six1, Ccnd2), NF-kappa B signaling pathway (Map3k7, Prkcb, Ikbkg), TNF signaling pathway (Map3k7, Ikbkg, Pik3ca), etc. (Fig. 5D). Furthermore, the transcription factor (TF)-gene interaction was conducted among the top 20 hub nodes in 5 mg and 25 mg SQ-diEG treated group (Fig. 5E). Interestingly, *Myc* and *Prdm1,* which activations have been studied for their significance in immune suppression [26, 27], were found to be significantly downregulated by SQ-diEG in the process of transcriptional regulation, and their gene expressions were validated by Rt-qPCR (Fig. 5F-I).

All in all, these results unraveled that both concentrations of SQ-diEG upregulated the apoptosis pathway and natural killer cell mediated cytotoxicity pathway. However, 5 mg SQ-diEG relatively improved more immune-related pathways, comparatively 25 mg SQ-diEG repressed more pathways correlated with the aggravation of melanoma metastasis.

Classification of the common regulated DEGs by SQ-diEG

Furthermore, we aimed to explore the common genes and their functions between 5 and 25 mg SQ-diEG in the context of melanoma metastasis. The Venn diagram showed that 45 genes were upregulated, and 128 genes were downregulated in both concentrations (Fig. 6A). These genes particularly participated in the upregulation of collagen biosynthesis (Hdac2, Runx1), activation of immune response (Ap1g1, Rabl3, Ikzf1, Pdgfra, Actr2, Il10rb, Plpp6, Atf7, Raf1, Cdk13, Skint1, Chst3), and the downregulation of inflammation mediated by chemokine and cytokine signaling pathway (Itgb2, Jak2, Ccr2), integrin signaling pathway (Parvb, Itgax, Rap2a) and cell–cell adhesion (Cadm2, Prdm1, Cdh7, Pycard, Srpx2, Bcl6, Myadm, Pkp1, Cdk5r1, Ibsp, Duox2) (Fig. 6B). Hence, these results displayed that SQ-diEG actively exerted its anti-metastatic role in a melanoma tumor-immune microenvironment through the stimulation of ECM remodeling and immune response, while the suppression of pro-tumorigenic genes in TME.

SQ-diEG may exert anti-melanoma effect through the activation of Caspases

The majority of the cytotoxic agents exert their anti-proliferative and anti-cancer effect by stressing the cancer cells through the activation of apoptosis, a programmed cell death that is lapsed in cancer cells [28]. Despite having observed a positive regulation of apoptosis and stress-related terms in vivo that perhaps were caused by SQ-diEG (Fig. 5A-D), to validate whether this apoptosis was directly in connection with the SQ-diEG cytotoxic-induced stress, we first examined the activity of major downstream effectors (Caspase 3 and 7) in apoptosis pathway by measuring the luminescence [29]. Our results exhibited that 2.5 μM and 40 μM of SQ-diEG significantly upregulated the Caspase 3/7 activity in murine B16F10 cells (Fig. 7A). Whereas, a higher concentration (30 μM) of SQ-diEG significantly upregulated the Caspase 3/7 activity in human skin SK-MEL-28 cells (Fig. 7B). These results revealed that apoptosis may be involved in the melanoma cells following SQ-diEG treatment. To further confirm the activity of SQ-diEG in apoptotic pathway, we examined the gene expression of fundamental regulators in the B-cell lymphoma 2 (Bcl-2) family, including *Bax* and *Bak* (apoptotic executor) and *Bcl-xL* (apoptotic inhibitor) which are known as apoptotic switches to initiate programmed cell death via the manipulation between their pro- and anti-survival functions [30]. Our results showed that SQ-diEG enhanced the transcriptional expression level of pro-apoptotic *Bax* and *Bak* and inhibited anti-apoptotic *Bcl-xL* in both B16F10 and SK-MEL-28 cells (Fig. 7C-E, H-J). In addition, aiming to understand if the apoptosis triggered in melanoma cells was because of the cytotoxic signals from SQ-diEG treatment, the expression of two major transcription factors (*Tp53* and *Atf4*), which not only play a central role in apoptosis as stress sensor but also act as tumor suppressor in many cancers, were checked via Rt-qPCR. Interestingly, we have discovered that SQ-diEG

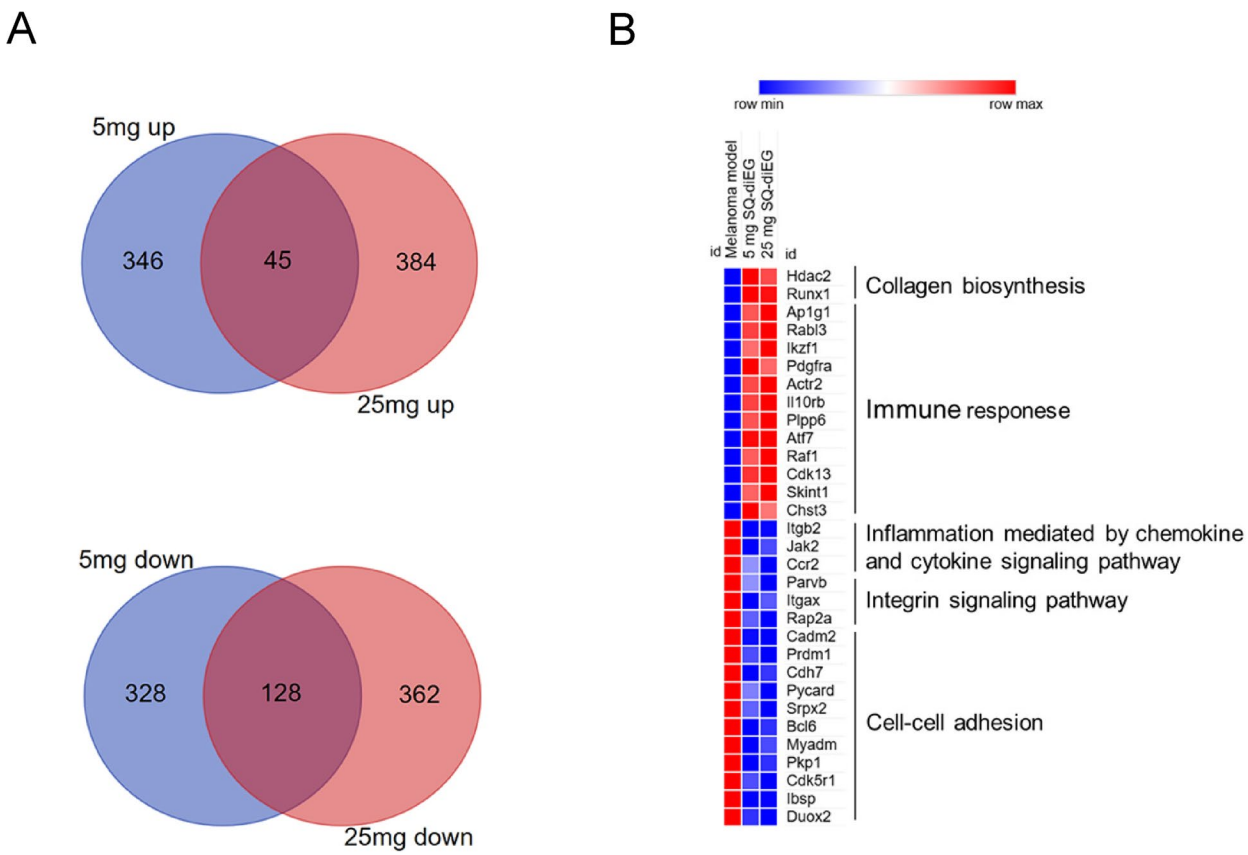

Fig. 6 Classification of common DEGs and categories of their functions in 5 mg and 25 mg SQ-diEG. **A** Venn diagram shows that 45 DEGs were upregulated by both 5 mg and 25 mg SQ-diEG; 128 DEGs were downregulated by both 5 mg and 25 mg SQ-diEG. **B** Heatmap shows the relative gene expression changes in SQ-diEG treatment groups. Significant genes were categorized according to their molecular functions

significantly upregulated the gene expression of *Tp53* and *Atf4* in both murine and human melanoma cells in a dose and time-dependent manner (Fig. 7F-G, K-L) Conceivably, these investigations pointed out that SQ-diEG, as a cytotoxic compound, exerts its anti-melanoma effect through the activation of programmed death in cancer cells and subsequently fewer cells were able to proliferate, disseminate and further colonize the lung in mice.

Discussion

Melanoma metastasis is an integral chain reaction which creates a dilemma making it extremely difficult to intervene the progression efficiently by drugs. The demands for anti-metastatic drugs with high efficacy are still urgently concerned [31]. In recent years, nanotechnology-based drug delivery systems (DDSs), including the polyethylene glycol (PEG)-coated amphiphilic nanoparticle,

(See figure on next page.)

Fig. 7 SQ-diEG induced apoptosis in melanoma cells by regulating mitochondria-dependent caspase activation pathway. **A** The effect of SQ-diEG on the activation of Caspase 3/7 activity in B16F10 cells. **B** The effect of SQ-diEG on the activation of Caspase 3/7 activity in SK-MEL-28 cells. **C** The effect of SQ-diEG on mRNA expression of pro-apoptotic gene marker *Bax* in B16F10 cells. **D** The effect of SQ-diEG on mRNA expression of pro-apoptotic gene marker *Bak* in B16F10 cells. **E** The effect of SQ-diEG on mRNA expression of anti-apoptotic gene marker *Bcl-xL* in B16F10 cells. **F** The effect of SQ-diEG on mRNA expression of transcription factor *Tp53* in B16F10 cells. **G** The effect of SQ-diEG on mRNA expression of transcription factor *Atf4* in B16F10 cells. **H** The effect of SQ-diEG on mRNA expression of pro-apoptotic gene marker *BAX* in SK-MEL-28 cells. **I** The effect of SQ-diEG on mRNA expression of pro-apoptotic gene marker *BAK* in SK-MEL-28 cells. **J** The effect of SQ-diEG on mRNA expression of anti-apoptotic gene marker *BCL-XL* in SK-MEL-28 cells. **K** The effect of SQ-diEG on mRNA expression of transcription factor *TP53* in SK-MEL-28 cells. **L** The effect of SQ-diEG on mRNA expression of transcription factor *ATF4* in SK-MEL-28 cells. All the data were analyzed and expressed as mean ± standard deviations (SD) ($n = 3$). The level of significance between two value sets (ctrl cells vs. treated cells) was determined by student's t test: * $P < 0.05$, ** $P < 0.01$, *** $P < 0.0001$

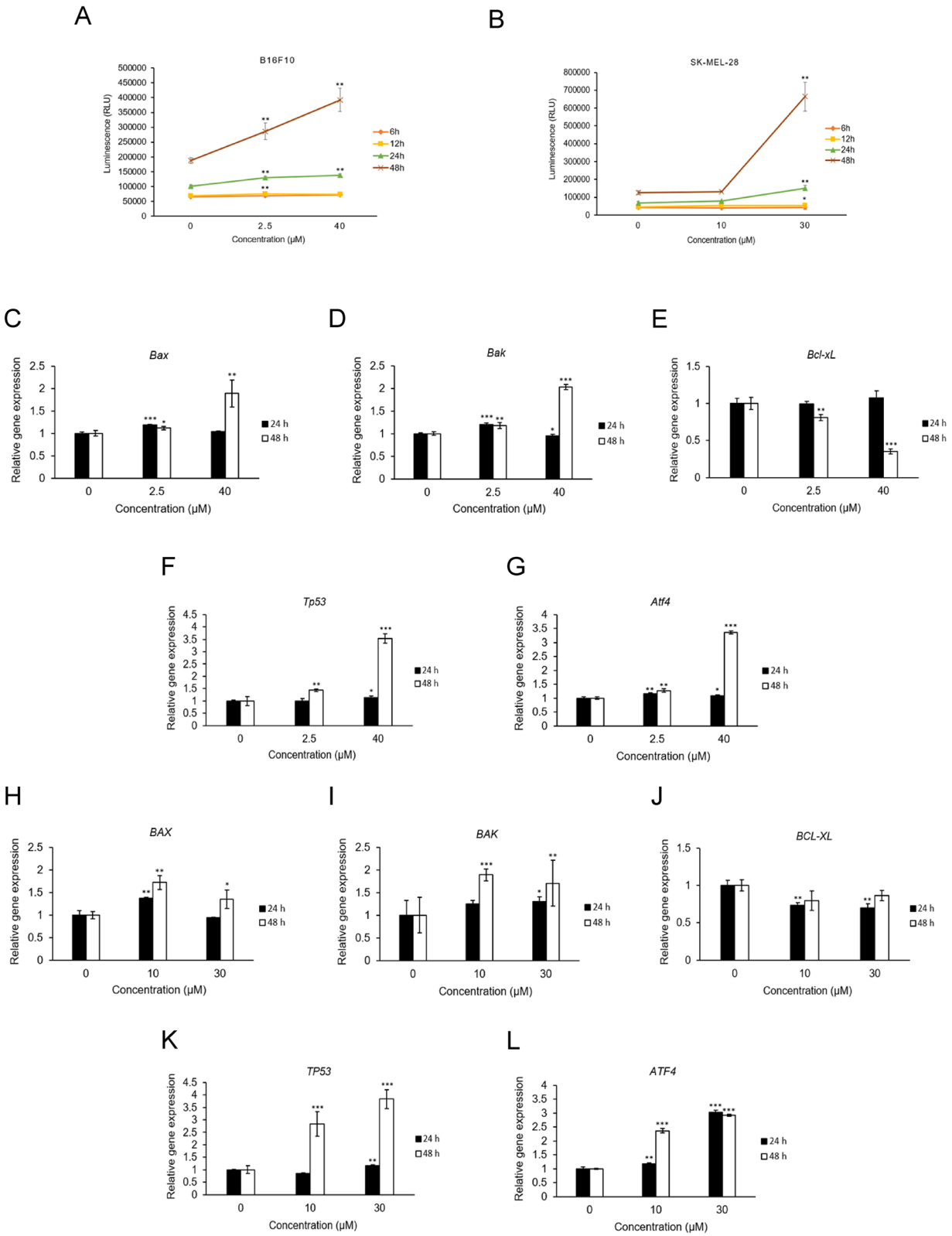

Fig. 7 (See legend on previous page.)

have been actively applied to overcome some difficulties in the discovery and development of novel anti-cancer drugs, such as low water solubility of the drug candidates, low aggregated concentration in tumor tissue, and therapeutic resistance, but without causing undue effects to normal cells [32, 33]. Though some lines of evidence suggesting SQ has suppressive effect on tumor growth [17], its pharmacological potentials in actual cancer environment have been largely underestimated, most likely due to the poor cell penetrability and low bioavailability which impede its way to reach the site of pathology [34]. A novel EG derivative of SQ has been recently discovered to form self-assembled vesicles to better incorporate into the surrounding polar environment with a higher amphiphilic activity and higher sensitivity [18]. In this present study, we demonstrated the effect of SQ-diEG as a potent drug molecule against the melanoma metastasis. The anti-metastatic like effect of SQ-diEG was discovered in malignant melanoma cells (Fig. 2A-F). In-vivo tumorigenesis assay suggested that administration of 25 mg SQ-diEG significantly ameliorated the tumor burden on the lung in B16F10 injected mice, indicating a potential anti-proliferative, anti-clonogenic and anti-metastatic activity of SQ-diEG in melanoma (Fig. 3B).

TME plays an indispensable role on immunosuppression, tumor proliferation, tissue invasion, metastatic dissemination as well as the development of drug resistance [35]. Extracellular proteinases, especially MMP2 and MMP9, are recognized as major modulators to mediate various events (tumor proliferation, angiogenesis, EMT, ECM destruction, etc.) in TME to support the melanoma metastasis [6, 36]. Thus, we examined the expression of MMP2 and MMP9 at the margin of melanoma tissue, where is considered the invasive part and to have the unique TME [37]. Results indicated that SQ-diEG suppressed the expression of MMP2 and MMP9 in tumor tissue (Fig. 3C, Fig. S3), and reduced the mRNA expression of several melanoma metastatic-associated markers including *Ikbke, Hmox1, Sqstm1, Mgp*, and *Nnmt* (Fig. 3D-H), which play a regulatory role not only on melanoma metastasis but also in TME in various type of cancers [38–44]. Moreover, the global gene profiling of melanoma tumor tissues revealed that SQ-diEG may play a certain role in interacting with both immune cells and tumors in a heterogenous microenvironment, but its activity varied according to dosage. Notably, a higher dose of SQ-diEG administration was discovered to behave better than a lower dose, probably due to the higher aggregated concentration in tumor tissue; thus, this may more effectively modulate the reconstruction of ECM structures and melanoma metastatic-correlated pathways in TME (Fig. 5B, D). In addition, among the top hub nodes, SQ-diEG significantly downregulated the *Myc* expression, which contributes profoundly to melanoma metastasis through oncogenic pathways and involves in the TME to prompt melanoma tumorigenesis by inducing immune evasion (Fig. 5E, F, H) [26, 45]. Inhibition of *Prdm1* expression and its related signaling pathways (e.g. PRDM1/BLIMP1 pathway) has been reported to be a novel strategy in immunotherapy [27, 46], whereas its expression was significantly reduced by SQ-diEG (Fig. 5E, G, I). Consecutively secretion of inflammatory chemokines and cytokines by immune cells and tumor cells shapes the TME to facilitate the melanoma metastasis [47]. A list of common genes which regulated by both concentrations of SQ-diEG showed upregulation of collagen synthesis and immune response while downregulation of inflammation mediated by chemokine and cytokine signaling pathway, and integrins and other cell adhesion molecules, demonstrating a potential therapeutic role of SQ-diEG in the context of melanoma TME (Fig. 6B).

The heterogeneity in melanoma tumors is hard to predict which showing the different pattern of proliferation rate and invasive phenotype among sub-populations [48]. Researchers have identified that melanoma with lower proliferation is characterized with higher invasive properties [49]. Interestingly, SQ-diEG suppressed both melanoma cell proliferation and migration/invasion in our results (Figs. 1B-H and 2A-F). Therefore, we hypothesized that as a cytotoxic molecule to melanoma cells, SQ-diEG may exerts cellular stress on tumor cells by causing cell death, consequently decreasing the number of tumor cells for dissemination and encroachment upon organs in mice (Fig. 3B). We have also found evidence in microarray analysis that SQ-diEG upregulated several stress-related GOs as well as the upregulation of apoptosis (Fig. 5A-D). In normal cases, cytotoxic drugs can stress cancer cells through intervening with the cell cycling [50]. According to our results, 48 h treatment of 40 μM SQ-diEG attenuated the cellular proliferation of B16F10 cells by inducing cell cycle arrest in S phase, while this arrest shifted to G0/G1 phase after 72 h (Fig. 1B-F). These observations supported that melanoma cells were undergoing internal repair by halting the cell cycling in S phase but extended exposure to SQ-diEG may further lead to the failure of cell cycle re-entry in G0/G1 phase where survived cells from the initial stress became more migrative and invasive to overcome self-destruction and develop drug resistance [51]. However, when cancer cells are kept blocked at a certain stage of the cell cycle, they will no longer be able to repair the DNA damage, and thus cell apoptosis will occur, and this phenomenon is considered to be one of the main strategies to prevent tumor malignancies [28, 52]. Moreover, mitochondria is not only closely related with the tumor

proliferation but also dynamically participated in the melanoma progression [23]. It has been widely discussed that higher mitochondrial membrane potential (Δψm) is a hallmark feature of the enhanced cancer cell survival, cancer stem-like behavior, secretion of collagen degrading MMPs and angiogenic factors, signifying a higher invasiveness in vitro and increased metastasis in vivo [53, 54]. While, the decrease in Δψm represents the happening of apoptosis [55]. The collapse of the ΔΨm triggers the opening of the mitochondrial permeability transition pores (MPTP) to release cytochrome C in the cytosol and finally activate the major downstream effectors, Caspase 3 and Caspase 7, to induce the apoptosis in cells [29, 56]. Release of cytochrome C is mainly initiated and executed by the balance between pro-apoptotic and anti-apoptotic members in the Bcl2 family [30]. Interestingly, we have observed that SQ-diEG significantly suppressed the mitochondrial membrane potential (Δψm) in SK-MEL-28 cells (Fig. 1H, Fig. S2) and activated the Caspase 3/7 activity in B16F10 and SK-MEL-28 cells (Fig. 7A, B). The upregulation of pro-apoptotic members *Bax* and *Bak* as well as the downregulation of anti-apoptotic member *Bcl-xL* (Fig. 7C-E, H-J) suggested that SQ-diEG may inhibit the melanoma cell proliferation and invasiveness through the mitochondria-mediated caspase activation apoptotic signaling pathway.

The tumor protein p53 (*Tp53)* transcription factor is considered the master senser of cellular stress that is caused by cytotoxic stimuli, such as cytotoxic drugs [57, 58]. When cancer cells are injured from stress, the *Tp53* is activated by DNA damage and can further transcriptionally activating pro-apoptotic Bcl2 family members and neutralizing anti-apoptotic Bcl2 proteins to initiate apoptosis [59]. The upregulation of *Tp53* expression in both melanoma cell lines indicated that SQ-diEG could directly exert pressure on melanoma cells and cause DNA damage inside of the cells (Fig. 7F, K). On the other hand, endoplasmic reticulum (ER) stress is an additional cell adaptation strategy in response to cellular stress, and it plays a significant role in the mitochondrial pathway of apoptosis by regulating crosstalk between mitochondria and the ER as well as the equilibrium between the positive and negative Bcl2 family members [60]. Activating transcription factor 4 (*Atf4*) is the major regulator of ER stress which can further mediate the pore activity of *Bax* and *Bak* on mitochondria membrane in response to stress to cause apoptosis [61, 62]. The enhanced expression of *Atf4* in both cell lines suggested a possible involvement of ER stress response following the treatment of SQ-diEG (Fig. 7G, L). Meanwhile, the impact of *Tp53* and *Atf4* is substantial reflected by their dual role in the cancer progression. Despite their functions in apoptosis, *Tp53* and *Atf4* have been extensively studied for their tumor suppressor role on cancer metastatic-associated activities, such as tumor proliferation, invasion and migration, hence making them attractive as promising drug targets [63–66].

Conclusion

Collectively, in this study we exhibited the suppressive role of a novel amphiphilic EG squalene derivative on melanoma malignancy by downregulating metastatic-associated biomarkers while concurrently inducing apoptosis in cancer cells through the mitochondria-dependent caspase activation pathway. The global gene expression profiling in melanoma tissues also revealed a potential role of SQ-diEG in TME which highlighted some possibilities of SQ-diEG in immunotherapy. Thus, we anticipate that this research may advance our understanding of and application for the SQ-based molecule as a promising medication option for the treatment of cancer.

Abbreviations

EMT	Epithelial-mesenchymal transition
ECM	Extracellular matrix
MMP	Matrix Metalloproteinase
TME	Tumor microenvironment
SQ	Squalene
SQ-diEG	2-[2-(2-Hydroxyethoxy)ethoxy]-3-hydroxysqualene
EG	Ethylene glycol
DTIC	Dacarbazine
DEGs	Differentially expressed genes
GOs	Gene ontologies
PPI	Protein-protein interaction
DDSs	Drug delivery systems
PEG	Polyethylene glycol
Ikbke	I-kappa-B kinase epsilon
Hmox1	Heme Oxygenase 1
Sqstm1	Sequestosome 1
Mgp	Matrix Gla protein
Nnmt	Nicotinamide N-methyltransferase
MPTP	Mitochondrial permeability transition pores
Bcl2	B-cell lymphoma 2
Bax	BCL-2-associated X protein
Bak	BCL2 Antagonist/Killer 1
Bcl-xL	B-cell lymphoma-extra large
ER	Endoplasmic reticulum
Tp53	Tumor protein P53
Atf4	Activating transcription factor 4

Supplementary Information

The online version contains supplementary material available at https://doi.org/10.1186/s12964-024-01813-5.

Supplementary Material 1.

Acknowledgements

We appreciate precise advice on mechanism of action by Professor Colin R. Goding of Oxford University in this study.

Authors' contributions

Y.Z. contributed to the experimental design and performed the experiments, data analysis and interpretation, prepared the figures, and wrote the manuscript. M.B. contributed to the experimental design and revised the manuscript. T.N.L. prepared the SQ-diEG sample and revised the manuscript. T.A. participated it in the data analysis, curation and validation of the sample,

and revised the manuscript. H.I. conceived and supervised the study, managed funding and resources for the study and reviewed the manuscript. All authors read and approved the final manuscript.

Funding
This study was supported by Program on Open Innovation Platform with Enterprises, Research Institute and Academia (OPERA) (Grant # JPMJOP1832), and JST COI-NEXT (grant number: JPMJPF2017).

Availability of data and materials
The data that support the findings of this study are available within the paper and in additional file. The microarray data have been deposited to NCBI, GEO database (accession: GSE263339) https://www.ncbi.nlm.nih.gov/geo/query/acc.cgi?acc=GSE263339.

Declarations

Competing interests
The authors declare no competing interests.

Received: 1 May 2024 Accepted: 31 August 2024
Published online: 11 September 2024

References

1. Saginala K, Barsouk A, Aluru JS, Rawla P, Barsouk A. Epidemiology of Melanoma Medical Sciences. 2021;9:63.
2. Gil D, Ciołczyk-Wierzbicka D, Dulińska-Litewka J, Żwawa K, McCubrey JA, Laidler P. The mechanism of contribution of integrin linked kinase (ILK) to epithelial-mesenchymal transition (EMT). Adv Enzyme Regul. 2011;51:195–207.
3. Koop S, MacDonald IC, Luzzi K, Schmidt EE, Morris VL, Grattan M, et al. Fate of Melanoma Cells Entering the Microcirculation: Over 80% Survive and Extravasate1. Can Res. 1995;55:2520–3.
4. Nicolson GL. Cancer metastasis: Organ colonization and the cell-surface properties of mallignant cells. Biochimica et Biophysica Acta (BBA) - Reviews on Cancer. 1982;695:113–76.
5. Mahabeleshwar GH, Byzova TV. Angiogenesis in Melanoma. Semin Oncol. 2007;34:555–65.
6. Kessenbrock K, Plaks V, Werb Z. Matrix Metalloproteinases: Regulators of the Tumor Microenvironment. Cell. 2010;141:52–67.
7. Hofmann UB, Westphal JR, van Muijen GNP, Ruiter DJ. Matrix Metalloproteinases in Human Melanoma. J Investig Dermatol. 2000;115:337–44.
8. Nobili S, Lippi D, Witort E, Donnini M, Bausi L, Mini E, et al. Natural compounds for cancer treatment and prevention. Pharmacol Res. 2009;59:365–78.
9. Kang T-H, Yoon G, Kang I-A, Oh H-N, Chae J-I, Shim J-H. Natural Compound Licochalcone B Induced Extrinsic and Intrinsic Apoptosis in Human Skin Melanoma (A375) and Squamous Cell Carcinoma (A431) Cells. Phytother Res. 2017;31:1858–67.
10. Sztiller-Sikorska M, Koprowska K, Majchrzak K, Hartman M, Czyz M. Natural Compounds' Activity against Cancer Stem-Like or Fast-Cycling Melanoma Cells. PLoS ONE. 2014;9: e90783.
11. Huang C-H, Lu S-H, Chang C-C, Thomas PA, Jayakumar T, Sheu J-R. Hinokitiol, a tropolone derivative, inhibits mouse melanoma (B16–F10) cell migration and in vivo tumor formation. Eur J Pharmacol. 2015;746:148–57.
12. Deng L-J, Qi M, Li N, Lei Y-H, Zhang D-M, Chen J-X. Natural products and their derivatives: Promising modulators of tumor immunotherapy. J Leukoc Biol. 2020;108:493–508.
13. Poornima P, Kumar JD, Zhao Q, Blunder M, Efferth T. Network pharmacology of cancer: From understanding of complex interactomes to the design of multi-target specific therapeutics from nature. Pharmacol Res. 2016;111:290–302.
14. Kaya K, Nakazawa A, Matsuura H, Honda D, Inouye I, Watanabe MM. Thraustochytrid *Aurantiochytrium* sp. 18W–13a Accummulates High Amounts of Squalene. Biosci Biotechnol Biochem. 2011;75:2246–8.
15. Kelly GS. Squalene and its potential clinical uses. Alternative medicine review: a journal of clinical therapeutic. 1999;4:29–36.
16. Ronco AL, Stéfani ED. Squalene: a multi-task link in the crossroads of cancer and aging. Functional Foods in Health and Disease. 2013;3:462.
17. Rao CV, Newmark HL, Reddy BS. Chemopreventive effect of squalene on colon cancer. Carcinogenesis. 1998;19:287–90.
18. Linh TN, Arimura T, Tominaga K, Kigoshi H, Isoda H. Syntheses and aggregation properties of new squalene receptors bearing open chain ligands. Supramol Chem. 2021;33:194–201.
19. Sherman BT, Hao M, Qiu J, Jiao X, Baseler MW, Lane HC, et al. DAVID: a web server for functional enrichment analysis and functional annotation of gene lists (2021 update). Nucleic Acids Res. 2022;50:W216–21.
20. Zhou Y, Zhou B, Pache L, Chang M, Khodabakhshi AH, Tanaseichuk O, et al. Metascape provides a biologist-oriented resource for the analysis of systems-level datasets. Nat Commun. 2019;10:1523.
21. Feitelson MA, Arzumanyan A, Kulathinal RJ, Blain SW, Holcombe RF, Mahajna J, et al. Sustained proliferation in cancer: Mechanisms and novel therapeutic targets. Semin Cancer Biol. 2015;35:S25–54.
22. Scholzen T, Gerdes J. The Ki-67 protein: from the known and the unknown. J Cell Physiol. 2000;182:311–22.
23. Theodosakis N, Micevic G, Kelly DP, Bosenberg M. Mitochondrial function in melanoma. Arch Biochem Biophys. 2014;563:56–9.
24. Zorova LD, Popkov VA, Plotnikov EY, Silachev DN, Pevzner IB, Jankauskas SS, et al. Mitochondrial membrane potential. Anal Biochem. 2018;552:50–9.
25. Lu P, Weaver VM, Werb Z. The extracellular matrix: A dynamic niche in cancer progression. J Cell Biol. 2012;196:395–406.
26. Dhanasekaran R, Deutzmann A, Mahauad-Fernandez WD, Hansen AS, Gouw AM, Felsher DW. The MYC oncogene — the grand orchestrator of cancer growth and immune evasion. Nat Rev Clin Oncol. 2022;19:23–36.
27. Shen L, Chen Q, Yang C, Wu Y, Yuan H, Chen S, et al. Role of PRDM1 in tumor immunity and drug response: a pan-cancer analysis. Front Pharmacol. 2020;11: 593195.
28. Kerr JFR, Winterford CM, Harmon BV. Apoptosis. Its significance in cancer and cancer Therapy. Cancer. 1994;73:2013–26.
29. Lakhani SA, Masud A, Kuida K, Porter GA, Booth CJ, Mehal WZ, et al. Caspases 3 and 7: Key Mediators of Mitochondrial Events of Apoptosis. Science. 2006;311:847–51.
30. Singh R, Letai A, Sarosiek K. Regulation of apoptosis in health and disease: the balancing act of BCL-2 family proteins. Nat Rev Mol Cell Biol. 2019;20:175–93.
31. Velho TR. Metastatic melanoma – a review of current and future drugs. Drugs Context. 2012;2012: 212242.
32. Senevirathne SA, Washington KE, Biewer MC, Stefan MC. PEG based anticancer drug conjugated prodrug micelles for the delivery of anti-cancer agents. J Mater Chem B. 2016;4:360–70.
33. Zhang X, Wang H, Ma Z, Wu B. Effects of pharmaceutical PEGylation on drug metabolism and its clinical concerns. Expert Opin Drug Metab Toxicol. 2014;10:1691–702.
34. Strandberg T, Tilvis R, Miettinen T. Metabolic variables of cholesterol during squalene feeding in humans: comparison with cholestyramine treatment. J Lipid Res. 1990;31:1637–43.
35. Spano D, Zollo M. Tumor microenvironment: a main actor in the metastasis process. Clin Exp Metastasis. 2012;29:381–95.
36. Hofmann UB, Eggert AAO, Blass K, Bröcker E-B, Becker JC. Expression of Matrix Metalloproteinases in the Microenvironment of Spontaneous and Experimental Melanoma Metastases Reflects the Requirements for Tumor Formation. Can Res. 2003;63:8221–5.
37. Yu D, Lai P, Yan T, Fang K, Chen L, Zhang S. Quantifying the Matrix Metalloproteinase 2 (MMP2) Spatially in Tissues by Probe via MALDI Imaging Mass Spectrometry. Front Chem. 2021;9: 786283.
38. Möser CV, Meissner M, Laarmann K, Olbrich K, King-Himmelreich TS, Wolters MC, et al. The protein kinase IKKepsilon contributes to tumour growth and tumour pain in a melanoma model. Biochem Pharmacol. 2016;103:64–73.
39. Yin M, Wang X, Lu J. Advances in IKBKE as a potential target for cancer therapy. Cancer Med. 2020;9:247–58.
40. Zerfaoui M, Toraih E, Ruiz E, Errami Y, Attia AS, Krzysztof M, et al. Nuclear Localization of BRAFV600E Is Associated with HMOX-1 Upregulation and Aggressive Behavior of Melanoma Cells. Cancers. 2022;14:311.
41. Karras P, Riveiro-Falkenbach E, Cañón E, Tejedo C, Calvo TG, Martínez-Herranz R, et al. p62/SQSTM1 Fuels Melanoma Progression by Opposing mRNA Decay of a Selective Set of Pro-metastatic Factors. Cancer Cell. 2019;35:46–63.e10.

42. Boström K, Zebboudj AF, Yao Y, Lin TS, Torres A. Matrix GLA Protein Stimulates VEGF Expression through Increased Transforming Growth Factor-β1 Activity in Endothelial Cells *. J Biol Chem. 2004;279:52904–13.
43. Gerarduzzi C, Hartmann U, Leask A, Drobetsky E. The Matrix Revolution: Matricellular Proteins and Restructuring of the Cancer Microenvironment. Can Res. 2020;80:2705–17.
44. Ganzetti G, Sartini D, Campanati A, Rubini C, Molinelli E, Brisigotti V, et al. Nicotinamide N-methyltransferase: potential involvement in cutaneous malignant melanoma. Melanoma Res. 2018;28:82.
45. Wu X, Nelson M, Basu M, Srinivasan P, Lazarski C, Zhang P, et al. MYC oncogene is associated with suppression of tumor immunity and targeting Myc induces tumor cell immunogenicity for therapeutic whole cell vaccination. J Immunother Cancer. 2021;9: e001388.
46. Li Q, Zhang L, You W, Xu J, Dai J, Hua D, et al. PRDM1/BLIMP1 induces cancer immune evasion by modulating the USP22-SPI1-PD-L1 axis in hepatocellular carcinoma cells. Nat Commun. 2022;13:7677.
47. Richmond A, Yang J, Su Y. The good and the bad of chemokines/chemokine receptors in melanoma. Pigment Cell Melanoma Res. 2009;22:175–86.
48. Hoek KS, Eichhoff OM, Schlegel NC, Döbbeling U, Kobert N, Schaerer L, et al. In vivo Switching of Human Melanoma Cells between Proliferative and Invasive States. Can Res. 2008;68:650–6.
49. Perego M, Maurer M, Wang JX, Shaffer S, Müller AC, Parapatics K, et al. A slow-cycling subpopulation of melanoma cells with highly invasive properties. Oncogene. 2018;37:302–12.
50. Shapiro GI, Harper JW. Anticancer drug targets: cell cycle and checkpoint control. J Clin Invest. 1999;104:1645–53.
51. Yano S, Miwa S, Mii S, Hiroshima Y, Uehara F, Yamamoto M, et al. Invading cancer cells are predominantly in G0/G1 resulting in chemoresistance demonstrated by real-time FUCCI imaging. Cell Cycle. 2014;13:953–60.
52. Chen J. The Cell-Cycle Arrest and Apoptotic Functions of p53 in Tumor Initiation and Progression. Cold Spring Harb Perspect Med. 2016;6: a026104.
53. Yadav UP, Singh T, Kumar P, Sharma P, Kaur H, Sharma S, et al. Metabolic Adaptations in Cancer Stem Cells. Front Oncol. 2020;10:1010.
54. Begum HM, Shen K. Intracellular and microenvironmental regulation of mitochondrial membrane potential in cancer cells. WIREs Mechanisms of Disease. 2023;15: e1595.
55. Ly JD, Grubb DR, Lawen A. The mitochondrial membrane potential (Δψm) in apoptosis; an update. Apoptosis. 2003;8:115–28.
56. Crompton M. The mitochondrial permeability transition pore and its role in cell death. Biochemical Journal. 1999;341:233–49.
57. Pflaum J, Schlosser S, Müller M. p53 Family and Cellular Stress Responses in Cancer. Front Oncol. 2014;4:285.
58. Herr I, Debatin K-M. Cellular stress response and apoptosis in cancer therapy. Blood. 2001;98:2603–14.
59. Mihara M, Erster S, Zaika A, Petrenko O, Chittenden T, Pancoska P, et al. p53 Has a Direct Apoptogenic Role at the Mitochondria. Mol Cell. 2003;11:577–90.
60. Szegezdi E, Logue SE, Gorman AM, Samali A. Mediators of endoplasmic reticulum stress-induced apoptosis. EMBO Rep. 2006;7:880–5.
61. Neill G, Masson GR. A stay of execution: ATF4 regulation and potential outcomes for the integrated stress response. Front Mol Neurosci. 2023;16:1112253.
62. Pihán P, Carreras-Sureda A, Hetz C. BCL-2 family: integrating stress responses at the ER to control cell demise. Cell Death Differ. 2017;24:1478–87.
63. Powell E, Piwnica-Worms D, Piwnica-Worms H. Contribution of p53 to metastasis. Cancer Discov. 2014;4:405–14.
64. Bagheri-Yarmand R, Williams MD, Grubbs EG, Gagel RF. ATF4 targets RET for degradation and is a candidate tumor suppressor gene in medullary thyroid cancer. J Clin Endocrinol Metab. 2017;102:933–41.
65. Chen J, Huang X, Zhang S, Zhu X. ATF4 inhibits tumor development and mediates p-GCN2/ASNS upregulation in colon cancer. Sci Rep. 2024;14:13042.
66. Armstrong JL, Flockhart R, Veal GJ, Lovat PE, Redfern CP. Regulation of endoplasmic reticulum stress-induced cell death by ATF4 in neuroectodermal tumor cells. J Biol Chem. 2010;285:6091–100.

Publisher's Note